

# Short wavelength ion temperature gradient instability in toroidal plasmas

Zhe Gao<sup>a)</sup>

Department of Engineering Physics, Tsinghua University, Beijing 100084, People's Republic of China

H. Sanuki and K. Itoh

National Institute for Fusion Science, Toki, Gifu 509-5292, Japan

J. Q. Dong

Southwestern Institute of Physics, Chengdu 610041, People's Republic of China

(Received 25 June 2004; accepted 5 November 2004; published online 10 January 2005)

Series of ion temperature gradient (ITG or  $\eta_i$ ) driven modes in the short wavelength region,  $|k_{\perp}\rho_i| > 1$ , are investigated with a gyrokinetic integral equation code in toroidal plasmas. These instabilities exist even if electrons are assumed adiabatic. However, nonadiabatic electron response can influence these short wavelength ITG (SWITG) modes, especially the fundamental  $l=0$  mode. At typical parameters, excitation of the  $l=0$  mode requires that both  $\eta_i$  and  $\eta_e$  exceed thresholds, while the  $l=1$  and  $l=2$  modes with higher harmonic eigenfunctions persist unstable even at  $\eta_e = 0$ . Dependence of the SWITG modes on other parameters is also investigated. The  $l=1$  mode with an odd potential eigenfunction grows faster than the  $l=0$  mode and may be dominant in low  $\eta_e$ , high  $\beta$ , weak positive magnetic shear, and/or weak toroidicity regions. © 2005 American Institute of Physics. [DOI: 10.1063/1.1840687]

## I. INTRODUCTION

Recently, intensive research attention is focused on understanding the anomalous electron transport in magnetically confined plasmas.<sup>1-4</sup> Experimental evidence<sup>5-7</sup> shows that this anomalous electron transport is governed by short wavelength turbulence, of course, after the stabilization of long wavelength turbulence. Moreover, observation of electron temperature profile stiffness in most experiments<sup>1</sup> indicates that the short wavelength instability responsible for electron transport should have a threshold in electron temperature gradient or  $1/L_{Te} \sim \nabla T_e/T_e$ .

Two kinds of instability are often considered to be candidates to explain electron transport in tokamak plasmas: the electron temperature gradient (ETG) modes and the trapped electron modes (TEMs). The TEMs have been well studied for years, usually with the coupling to ion temperature gradient (ITG) modes consideration.<sup>8,9</sup> The ITG-TEMs are characterized by long wavelength  $k_{\perp}\rho_i \ll 1$  and can induce electron transport with a mixing length estimated coefficient  $v_{ii}\rho_i^2/L_n$ . However, the turbulence induced by long wavelength instability is easily suppressed by the  $\mathbf{E} \times \mathbf{B}$  flow shear.<sup>10</sup> In recent years, numerous studies are performed on the ETG instabilities.<sup>11-13</sup> The ETG modes are unstable in the very short wavelength region  $k_{\perp}\rho_e \sim 1$ . However, nonlinear gyrokinetic simulations<sup>14</sup> show that ETG turbulence can also yield a large electron heat flux through radially highly elongated vortices. Both the ETG modes and TEMs can provide a threshold in electron temperature gradient, but the threshold depend on different parameters: temperature ratio  $T_e/T_i$  and ratio of magnetic shear to safety factor  $\hat{s}/q$  for ETG modes,<sup>11,12</sup> scale length of density profile and fraction of trapped electrons for TEMs.<sup>9</sup> Comparisons between ex-

periment results and theory model are also performed.<sup>1</sup> Some results seem to agree with the ETG model, such as the  $\hat{s}/q$  dependence of  $(1/L_{Te})_c$  in Tore Supra,<sup>15</sup> and some results show good agreement with the ITG/TEM model, such as the modulated electron temperature profile evolution in the ASDEX-Upgrade tokamak (axially symmetric divertor experiment).<sup>16</sup>

On the other hand, the electron transport might be controlled by multisource instabilities simultaneously or by different instability depending on different discharge condition. The case is more complicated when the ion and electron contribution cannot be absolutely separated. Results in the Joint European Torus (JET) (Ref. 5) have shown the link between long and short wavelength density fluctuation, and the ion and electron transport channels. In the tokamak fusion test reactor (TFTR), a similar link has also been observed, and the measured high  $k$  fluctuations propagate in the ion diamagnetic direction ( $\omega_r < 0$ ).<sup>6</sup>

Recently, an unstable mode driven by temperature gradients is identified by Smolyakov *et al.*<sup>17</sup> in the short wavelength region  $|k_y\rho_i| \gg 1$  in a shearless slab configuration. This mode propagates in the ion diamagnetic direction and seems to be a continuous extension of the conventional ( $|k_y\rho_i| \ll 1$ ) ITG mode, so called the short wavelength ITG (SWITG) mode. Our recent work<sup>18</sup> confirms that this "double-humped" behavior in the growth rate can be attributable to the Landau damping/resonance mechanism and the nonmonotonic behavior of the real frequency as  $k_y$  varies. We have also identified a series of SWITG modes with even or odd eigenfunction, respectively, with an integral eigenmode equation code in a sheared slab configuration. The fundamental even mode is excited by both finite  $\eta_i$  and  $\eta_e$ , hardly stabilized by  $\beta$ , but stabilized by magnetic shear. The odd mode has a higher growth rate in low  $\beta$  and weak magnetic shear regions. The radial widths of the SWITG modes are found to be compa-

<sup>a)</sup>Electronic mail: gaozhe@mail.tsinghua.edu.cn

rable with the conventional ITG modes, so the turbulence driven by SWITG instabilities can produce a significant level of transport. Hirose *et al.*<sup>19</sup> also indicate the existence of a temperature gradient driven mode in the short wavelength region in toroidal plasmas. This toroidal mode also requires both finite  $\eta_i$  and  $\eta_e$  for excitation. Parallel electron transit effect is conjectured<sup>19</sup> to provide destabilization, which is not consistent with the physical mechanism we discussed<sup>18</sup> in the sheared slab configuration. Also, the magnetic shear is reported destabilizing for the toroidal mode there and high order modes are not mentioned in this toroidal work.

In this paper, we employ a set of integral eigenvalue equation for the further study of toroidal SWITG modes. The magnetic curvature and gradient drift, the transit effect, and the finite Larmor radius effects are retained in the model for both electron and ions. Also, the electron response is easily switched to be adiabatic. Using this model, we would like to investigate the SWITG modes in detail. The physical driving mechanism in the toroidal geometry will be discussed with comparison with that in the sheared slab configuration. Higher order modes will be introduced and parameter dependence of the toroidal SWITG modes will be investigated in wider parameter regions. This work is an essential preparation for estimating the critical temperature gradient and possible transport driven by the SWITG instability.

The organization of this paper is as follows. The integral eigenmode equations are presented in Sec. II. Numerical results and analyses are described in Sec. III. Section IV is devoted to conclusions and discussion.

## II. INTEGRAL EIGENMODE EQUATION FORMALISM

The ballooning representation for an axisymmetric toroidal geometry with circular flux surface is employed. The  $s$ - $\alpha$  equilibrium model is applied. The derivation of the integral eigenmode equation had been given in many previous works<sup>20</sup> but still will be outlined here for the convenience of the following discussion. The magnetic curvature and gradient drift, the transit effect, and the finite Larmor radius effect are all retained for both ions and electrons, but the trapped particle effect is neglected.

The dynamics of low frequency electromagnetic perturbation in low- $\beta$  plasmas is described by the Poisson's equation

$$-k_{\perp}^2 \tilde{\phi} = -4\pi \sum_{j=i,e} q_j \int f_j d^3v \quad (1)$$

and the parallel component of the Ampère's law

$$-k_{\perp}^2 \tilde{A}_{\parallel} = -\frac{4\pi}{c} \sum_{j=i,e} q_j \int v_{\parallel} f_j d^3v \quad (2)$$

with

$$f_j = -\frac{q_j F_{Mj}}{T_j} \tilde{\phi}(\theta) + h_j(v_{\perp}, v_{\parallel}, \theta) J_0(\delta_j). \quad (3)$$

The nonadiabatic response  $h_j(v_{\perp}, v_{\parallel}, \theta)$  is determined from the gyrokinetic equation in ballooning space,

$$\left( \omega - \omega_{Dj} + i \frac{v_{\parallel}}{qR} \frac{\partial}{\partial \theta} \right) h_j = \frac{q_j F_{Mj}}{T_j} (\omega - \omega_{*j}^T) \times \left( \hat{\phi} - \frac{v_{\parallel}}{c} \hat{A}_{\parallel} \right) J_0(\delta_j), \quad (4)$$

where

$$\omega_{Dj} = \hat{\omega}_{Dj} \left( \frac{v_{\perp}^2}{2v_{ij}^2} + \frac{v_{\parallel}^2}{v_{ij}^2} \right),$$

$$\hat{\omega}_{Dj} = 2\epsilon_n \omega_{*j} [\cos \theta + \sin \theta (\hat{s}\theta - \alpha \sin \theta)],$$

$$\omega_{*j}^T = \omega_{*j} \left[ 1 + \eta_j \left( \frac{v_{\perp}^2}{v_{ij}^2} - \frac{3}{2} \right) \right],$$

$$k_{\perp}^2 = k_{\theta}^2 [1 + (\hat{s}\theta - \alpha \sin \theta)^2],$$

with

$$\delta_j = k_{\perp} \rho_j, \quad \rho_j = \frac{v_{ij}}{\Omega_j}, \quad v_{ij} = \sqrt{\frac{2T_j}{m_j}}, \quad \Omega_j = \frac{q_j B}{m_j c},$$

$$\omega_{*j} = \frac{c T_j k_{\theta}}{q_j B L_n},$$

$$L_n = -\left( \frac{1}{n} \frac{dn}{dr} \right)^{-1}, \quad \epsilon_n = \frac{L_n}{R}, \quad \eta_j = \frac{d \ln T_j}{d \ln n},$$

$$\hat{s} = \frac{r}{q} \frac{dq}{dr}, \quad \alpha = -q^2 R \frac{d\beta}{dr}, \quad \beta = \beta_i + \beta_e,$$

$$\beta_j = \frac{8\pi n T_j}{B^2}, \quad F_{Mj} = \frac{n_j}{\pi^{3/2} v_{ij}^3} \exp\left(-\frac{v^2}{v_{ij}^2}\right),$$

$q$  is the safety factor and  $J_0$  is the Bessel function of zero order. The well-known ballooning representation

$$\tilde{f} = \sum_{m=-\infty}^{+\infty} e^{im\theta} \int_{-\infty}^{+\infty} e^{-im\theta'} e^{-in(\zeta - q\theta')} e^{-i\omega t} \hat{f}(\theta') d\theta' \quad (5)$$

has been used in deriving Eq. (4) and the  $s$ - $\alpha$  equilibrium model with circular flux surface has been employed.

When the trapped particle effect is not considered, Eq. (4) can be easily integrated with the boundary condition  $h_j(\theta) = 0$  as  $|\theta| \rightarrow \infty$ . Substituting the integral form of  $h_j(\theta)$  into Eqs. (1) and (2), we obtain the following coupled integral eigenmode equations:

$$\left( 1 + Z_i \tau_i + \frac{k_{\perp}^2 \Omega_e^2}{2 \omega_p^2} \right) \hat{\phi} = \sum_{j=i,e} \int_{-\infty}^{+\infty} \frac{dk'}{\sqrt{\pi}} \times [H_j^{00}(k, k') \hat{\phi} + H_j^{01}(k, k') \hat{A}_{\parallel}], \quad (6)$$

$$-\frac{k_{\perp}^2}{2\beta_e} \hat{A}_{\parallel} = \sum_{j=i,e} \int_{-\infty}^{+\infty} \frac{dk'}{\sqrt{\pi}} [H_j^{01}(k, k') \hat{\phi} + H_j^{02}(k, k') \hat{A}_{\parallel}], \quad (7)$$

where  $\hat{\phi}(k)$  and  $\hat{A}_{\parallel}(k)$  are the extended Fourier components in ballooning space of  $\tilde{\phi}(r)$  and  $-v_{te} \tilde{A}(r)/c$ , and

$$H_j^{00} = i\sqrt{\tau_j M_j \text{sign}(q_j)} \int_{-\infty}^0 \frac{d\tau \exp(-i\omega\tau)}{2\tau L_s \lambda_j} \times \exp\left[-\frac{(k-k')^2}{4\tau^2 L_s^2} \tau_j M_j a_j\right] \left\{ \omega \tau_j Z_j - 1 + \frac{3}{2} \eta_j - \frac{\eta_j}{\lambda_j^2} \left( \lambda_j - b_{aj} + b_{gj} \frac{I_{1j}}{I_{0j}} \right) - \frac{\eta_j (k-k')^2}{4\tau^2 L_s^2} \tau_j M_j \right\} \Gamma_{0j}, \quad (8)$$

$$H_j^{01} = \frac{-1}{2\tau L_s} (k-k') H_j^{00}, \quad (9)$$

$$H_j^{02} = \frac{1}{(2\tau L_s)^2} (k-k')^2 H_j^{00} \quad (10)$$

with

$$a_j = 1 - i \frac{2\epsilon_n \tau g(\theta, \theta')}{(\theta - \theta')} \tau_j Z_j, \quad \lambda_j = \frac{1 + a_j}{2},$$

$$g(\theta, \theta') = (\hat{s} + 1)(\sin \theta - \sin \theta') - \hat{s}(\theta \cos \theta - \theta' \cos \theta') - \frac{\alpha}{2} [(\theta - \theta') - \sin(\theta - \theta')],$$

$$\Gamma_{0j} = I_{0j} \left( \frac{b_{gj}}{\lambda_j} \right) \exp\left(-\frac{b_{aj}}{\lambda_j}\right), \quad b_{gj} = \frac{k_{\perp} k'_{\perp}}{2} \left( \frac{M_j}{\tau_j Z_j^2} \right),$$

$$b_{aj} = \frac{(k_{\perp}^2 + k'_{\perp}{}^2)}{4} \left( \frac{M_j}{\tau_j Z_j^2} \right),$$

$$k = k_{\theta} \hat{s} \theta, \quad k' = k_{\theta} \hat{s} \theta', \quad L_s = \frac{\epsilon_n \hat{s}}{q}, \quad \omega_{pe}^2 = \frac{4\pi n e^2}{m_e},$$

$$\tau_j = \frac{T_e}{T_j}, \quad M_j = \frac{m_j}{m_e}, \quad Z_j = \frac{|q_j|}{e}.$$

We have normalized the wave numbers,  $k_{\theta}$ ,  $k$ , and  $k'$  to  $\rho_e^{-1}$ ; the frequency  $\omega$  to  $\omega_{*e}$ ; and the integral interval  $\tau$  to  $\omega_{*e}^{-1}$ , respectively.  $I_n$  is the modified Bessel function of order  $n=0,1$ , and  $\text{sign}(q_j)$  equals unity for electron species and minus unity for ion species. Also, we define  $M=M_i/1836$ ,  $Z_{eff}=Z_i$  for convenience in the following.

### III. NUMERICAL RESULTS AND ANALYSES

Equations (6) and (7) are solved numerically with the gyrokinetic integral equation code HD7. Previous results of ETG (Ref. 12) and ITG (Ref. 13) modes can be recovered from the integral equations presented here when ions and electrons are assumed to be adiabatic, respectively. Also, results from Hirose *et al.*<sup>19</sup> can be repeated, for example, the normalized eigenfrequency for default parameters in Ref. 19 is  $-0.25 + i0.067$  and our calculation gives  $-0.25 + i0.069$ . The numerical parameters, especially the maximum  $|\theta|$ , are checked to ensure numerical convergence. As we will show in the following discussion, the broaden  $|\theta|$  region causes more calculation needed for the SWITG mode than for conventional ITG or ETG modes.

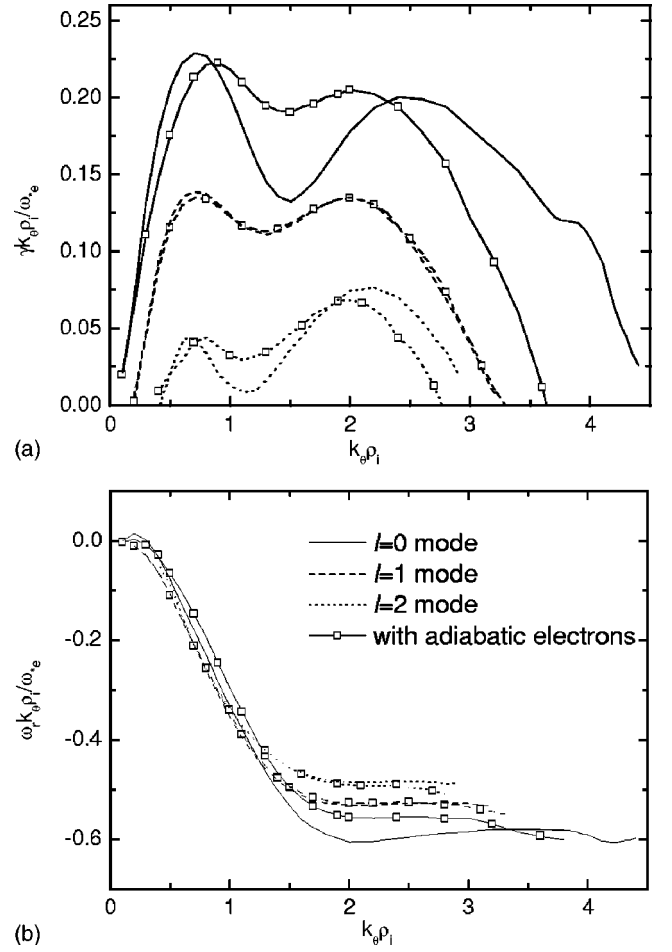


FIG. 1. Normalized growth rate (a) and frequency (b) vs  $k_{\theta} \rho_i$  for  $\eta_e=2.5$ ,  $\eta_i=2.5$ ,  $\tau_i=M=Z_{eff}=1$ ,  $\hat{s}=0.8$ ,  $q=1.5$ ,  $\epsilon_i=0.1$ , and  $\beta_e=0$ . The solid, dashed, dotted lines denote the different harmonic modes with  $l=0, 1$ , and  $2$ , respectively. The lines with squares are the corresponding results when electrons are assumed adiabatic.

The parameters for the numerical results given here are  $\eta_e=2.5$ ,  $\eta_i=2.5$ ,  $\tau_i=M=Z_{eff}=1$ ,  $\hat{s}=0.8$ ,  $q=1.5$ ,  $\epsilon_n=0.1$ ,  $\beta_e=0$ ,  $\Omega_e^2/\omega_p^2=0$ , and  $k_{\theta} \rho_i=2$  ( $k_{\theta} \rho_e=2/\sqrt{1836}$ ) unless otherwise stated.

#### A. Mode spectrum

The normalized mode growth rate and frequency multiplied with  $k_{\theta} \rho_i$  vs  $k_{\theta} \rho_i$  are shown in Fig. 1. Three unstable branches are presented with or without nonadiabatic electron effects consideration, respectively. As  $k_{\theta} \rho_i$  increases, the growth rate behaves double humps: the first peak at  $k_{\theta} \rho_i \approx 1$  is the conventional ITG mode, and the second peak at  $k_{\theta} \rho_i > 1$  is the short wavelength ITG (SWITG) mode. The unstable SWITG mode still exists even with adiabatic electron assumption. It implies that the ion contribution is essential for the SWITG mode although the electron response can influence the mode especially at large  $k_{\theta} \rho_i$ . In fact, the analytical discussion<sup>18</sup> for the slab mode indicates that the nonadiabatic electron response is about proportional to  $-i\pi^{1/2} \omega_{*e} / k_{\parallel} v_{te} (1 - \eta_e/2)$ .

Hirose *et al.*<sup>19</sup> had also identified the fundamental  $l=0$  mode in the toroidal configuration. In this paper, the behavior

of real frequency is well consistent with theoretical analysis, but it is conjectured that the SWITG instability is destabilized by the parallel electron transit effect. It seems not to be the case because the SWITG instability still exists in case of adiabatic electrons. In our earlier work<sup>18</sup> in a sheared slab configuration, a series of SWITG modes are found and investigated. We consider that the double-humped behavior in the growth rate of ion modes can be attributable to the non-monotonic behaviors of the real frequency as  $k_{\perp}$  varies, although electron kinetics can influence the mode in short wavelength regions. So it might be useful to compare the toroidal SWITG mode with the slab mode.

From Eq. (4), we can get the local ( $k_{\parallel}=\text{const}$ ) electrostatic response of ions

$$f_i = -\frac{q_i F_{Mi}}{T_i} \hat{\phi} + \frac{q_i F_{Mi}}{T_i} \left( \frac{\omega - \omega_{*i}^T}{\omega - \omega_{Di} - k_{\parallel} v_{\parallel}} \right) J_0^2(\delta_i) \hat{\phi}, \quad (11)$$

and its rough integral<sup>19</sup> for  $\omega_{*i} > \omega > (\omega_{Di} + k_{\parallel} v_{\parallel})$  yields

$$\bar{n}_i = \frac{-q_i \hat{\phi}}{T_i} n_0 + \frac{q_i \hat{\phi} \omega_{*i} (\eta_i/2 - 1)}{T_i \omega} I_0(b_i) \exp(-b_i). \quad (12)$$

If electrons are adiabatic, the following mode exists from the quasineutrality condition:

$$\omega = \left( \frac{\tau_i Z_{eff}}{\tau_i Z_{eff} + 1} \right) \left( \frac{\eta_i}{2} - 1 \right) \omega_{*i} I_0(b_i) \exp(-b_i). \quad (13)$$

Since  $\omega_{*i} = (-v_{ti}/L_n) \sqrt{b_i/2}$ , the real frequency increases with  $\sqrt{b_i}$  (or  $k_{\theta}$ ) in small  $b_i$  regions and tends to be constant in large  $b_i$  regions due to  $I_0(b_i) \exp(-b_i) \rightarrow 1/\sqrt{2\pi b_i}$  as  $b_i \rightarrow +\infty$ . This analytic result quite agrees with the numerical result and is well given by Hirose *et al.*<sup>19</sup> However, in the above derivation from Eqs. (11)–(13), we considered the real frequency only and the resonance mechanism have not been considered yet. From Eq. (11), we can see different resonance mechanisms in the slab and toroidal configurations. In the slab configuration, the magnetic drift does not exist and the Landau resonance/damping mechanism works at  $\omega \sim k_{\parallel} v_{ti}$ . When the real frequency approaches to a critical value  $(\omega/k_{\parallel} v_{ti})_c$ , the growth rate reaches its maximum. Since  $k_{\parallel} = k_y x/L_s$ , the normalized frequency  $\omega/k_{\parallel} v_{ti}$  is nonmonotonic, increasing at first and decreasing finally as  $k_y$  increases. If the maximum of  $\omega/k_{\parallel} v_{ti}$  is large enough, the  $\omega/k_{\parallel} v_{ti}$  will pass the critical value twice. This nonmonotonic behavior of  $\omega/k_{\parallel} v_{ti}$  results in the double-humped growth rate: the conventional ITG mode and the SWITG mode, which has been discussed in our earlier slab work.<sup>18</sup> In the toroidal geometry, the resonance mechanism changes but is similar. The ion transit term in toroidal geometry ( $k_{\parallel} v_{ti} \sim v_{ti}/qR$ ) is rather smaller than the magnetic drift term ( $\omega_{Di} \sim \epsilon_n \omega_{*i}$ ) at present parameters. Therefore, the toroidal mode is destabilized mostly by the magnetic drift resonance at  $\omega \sim \omega_{Di}$  (Ref. 21). Similar as the slab case, the normalized frequency  $\omega/\omega_{Di}$  increases with  $k_{\theta}$  in small  $k_{\theta}$  regions and decreases finally in large  $k_{\theta}$  regions due to  $\omega_{Di} \propto k_{\theta}$ . As a result, there are also two peaks in the growth rate, as shown in Fig. 1.

The stabilization effect of large  $k_{\theta}$  is also similar for the slab and toroidal mode. When  $k_{\theta}$  is so large that  $\omega_{Di}$  is much

larger than  $\omega$ , the ion nonadiabatic response will decay according to  $(R/L_n) I_0(b_i) \exp(-b_i)$  as  $b_i$  increases. Then the SWITG will be stable in very large  $k_{\theta}$  regions. For the slab mode, the similar stabilizing effect of large  $k_y$  is introduced by  $k_{\parallel} = k_y x/L_s$ , so the ion nonadiabatic response will decrease with about  $(L_s/L_n) I_0(b_i) \exp(-b_i)$  as  $b_i$  increases. The parameters we chose here and in the slab work are  $R/L_n = 10$  and  $L_s/L_n = 40$ , so the nonadiabatic response in the slab is larger than in the toroidal geometry. This might be why the toroidal SWITG mode has a narrower  $k_{\theta}$  spectrum than the slab mode. Also, in larger  $k_{\theta}$  regions, electron contribution becomes more important. In the local model, the  $k_{\parallel}$  is fixed, so the SWITG mode cannot be stabilized at large  $k_{\theta}$  if electron nonadiabatic contribution is not included.<sup>17</sup> The influence of electron kinetics on the slab SWITG mode has already been discussed in our earlier work.<sup>18</sup>

## B. Mode eigenfunction

Figures 2(a)–2(c) show eigenfunctions for three modes for  $k_{\theta} \rho_i = 2$ : even  $\phi(\theta)$  for the  $l=0$  and  $l=2$  modes; and odd  $\phi(\theta)$  for the  $l=1$  mode. The central part of the eigenmode is zoomed in and simultaneously plotted in Figs. 2(a)–2(c), respectively. Contrastively, the eigenfunctions from the adiabatic electron model are shown in Figs. 2(d)–2(f). The nonadiabatic electron effect hardly changes the central part,  $|\theta| < 4$ , of the eigenfunctions except the real part of the eigenfunction for the  $l=0$  mode. However, the localization of the eigenmode in the ballooning space is strongly influenced by the nonadiabatic electron effect. Obviously, if the adiabatic electron assumption is adopted, the eigenfunctions are rather smooth and localized in  $\theta$  space. When the nonadiabatic electron kinetics is considered, however, the eigenfunctions have broad structures along the magnetic field line and have oscillatory tails with a periodicity about  $\pi$ . This long tail structure might be explained by the electron kinetic effect through the term  $k_{\perp}^2 \rho_j^2 = k_{\theta}^2 \rho_j^2 (1 + \delta^2 \theta^2)$  within the finite Larmor radius effect term  $J_0$  in Eq. (4). As  $k_{\perp}^2 \rho_j^2$  increases with  $\theta$ , the ion or electron response decreases with the decay of  $J_0$  (strictly, its envelope). Since  $k_{\theta}^2 \rho_e^2 \ll 1$ ,  $k_{\perp}^2 \rho_e^2$  becomes large enough only in the large  $\theta$  regime. In other words, the electron kinetic response has a much broader spectrum in the ballooning space than the ion response. If we use the formula

$$\langle \theta^2 \rangle = \frac{\int \theta^2 |\phi(\theta)|^2 d\theta}{\int |\phi(\theta)|^2 d\theta} \quad (14)$$

to estimate the localization of the eigenmode in the ballooning space,  $\sqrt{\langle \theta^2 \rangle_{na}}$  for nonadiabatic electron case is 6.44, about 16 times of  $\sqrt{\langle \theta^2 \rangle_a}$  for adiabatic electron case. In fact, the nonadiabatic electron effect also strongly influences the eigenfunction for the conventional ITG mode in the  $k_{\theta} \rho_i \lesssim 1$  regime, although the eigenfrequency is slightly influenced. In addition, the oscillation in the tail leads to a large expenditure of computer time. The maximum  $|\theta|$  we used in calculations is 57.5 and the modes converge at about  $|\theta| \geq 40$ .

## C. Temperature gradient dependence

Dependence of the growth rate on  $\eta_i$  is shown in Fig. 3(a) for  $\eta_e = 2.5$ . Each of the three modes has a  $\eta_i$  threshold,

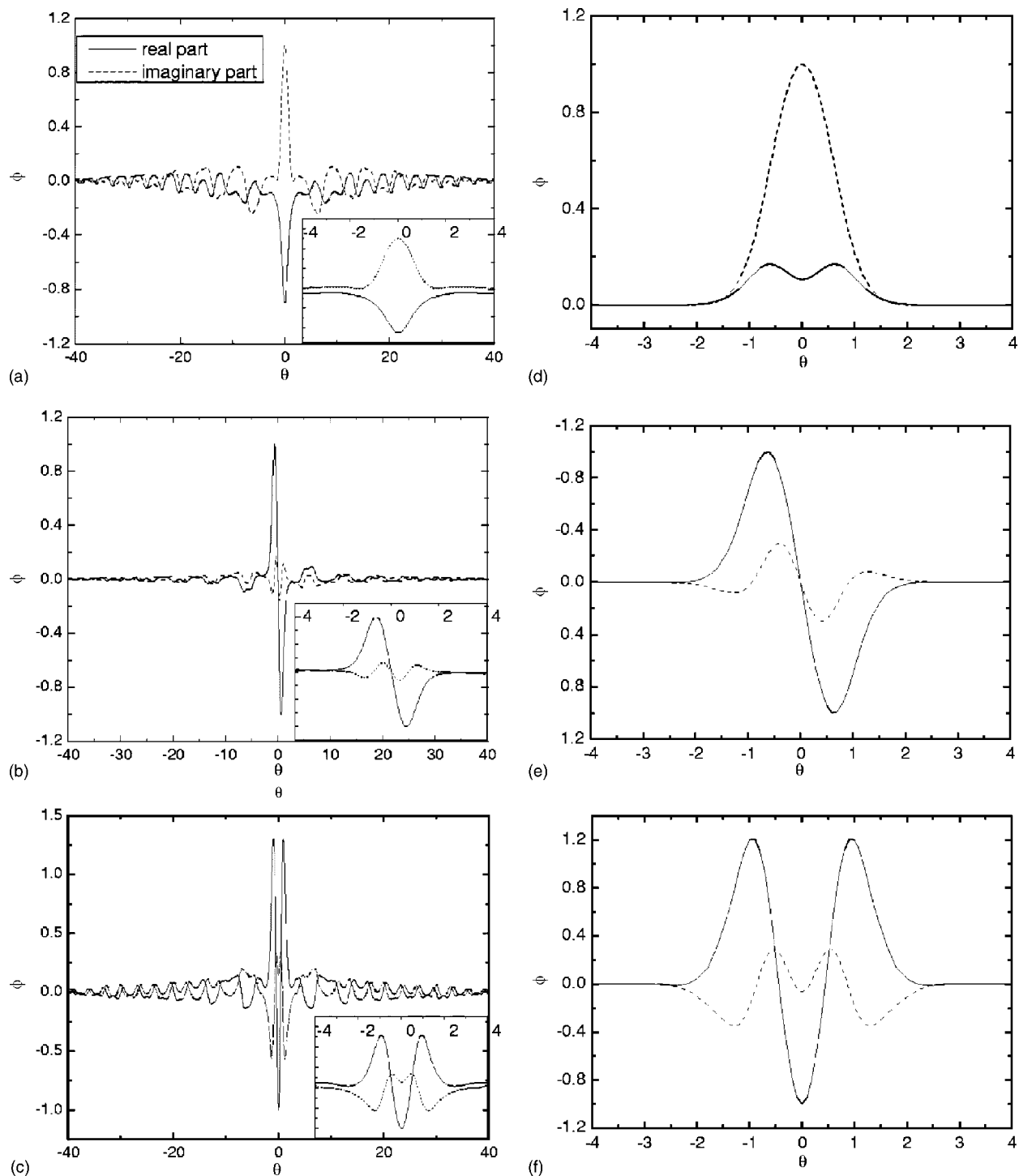


FIG. 2. Eigenfunction  $\hat{\phi}(\theta)$  for the  $l=0$  [(a) and (d)], 1 [(b) and (e)], and 2 [(c) and (f)] modes for  $k_{\theta}\rho_i=2$ . (a), (b), and (c) are from the nonadiabatic electron model, and (d), (e), and (f) are from the adiabatic electron model. The central part of the eigenfunctions from the nonadiabatic electron model is also zoomed in and pasted in the corners of (a), (b), and (c), respectively. Other parameters are the same as in Fig. 1.

which implies the essential of ion temperature gradient driven modes. The  $\eta_i$  threshold of the fundamental mode is lower than those of higher order modes.

Figure 3(b) shows the growth rate as function of  $\eta_e$  for  $\eta_i=2.5$ . Previous studies<sup>18,19</sup> indicate that the SWITG mode is unstable when both  $\eta_i$  and  $\eta_e$  exceed thresholds. This conclusion is still valid for the fundamental mode, but not for the higher order modes. The  $l=1$  and  $l=2$  modes persist unstable even  $\eta_e$  decreases to zero.

Temperature gradient dependence of the  $l=0$  and  $l=1$  modes for  $k_{\theta}\rho_i=2$  is more clearly demonstrated in Fig. 3(c). Three critical lines divide the  $\eta_i$ - $\eta_e$  diagram into five regions: both  $l=0$  and  $l=1$  modes are stable in the region "A;" the  $l=0$  mode is unstable in the regions "B," "C," and "D;" and the  $l=1$  mode is unstable in the regions "C," "D," and "E." Obviously, electron kinetics strongly influences the  $l=0$  mode, so excitation of the  $l=0$  mode requires that  $\eta_e$  exceed a threshold. Contrastively,  $\eta_e$  only slightly influences

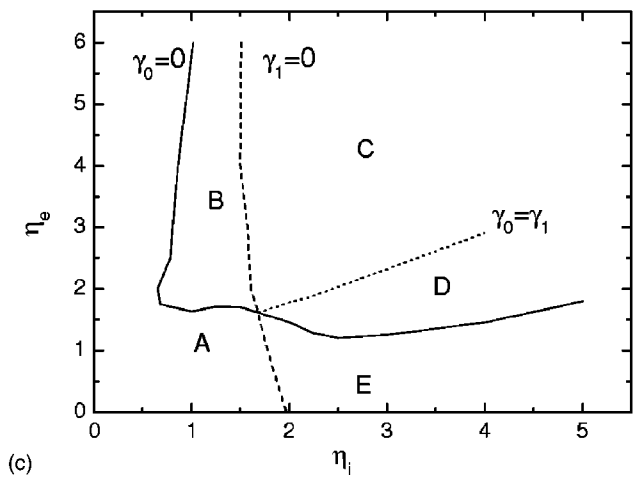
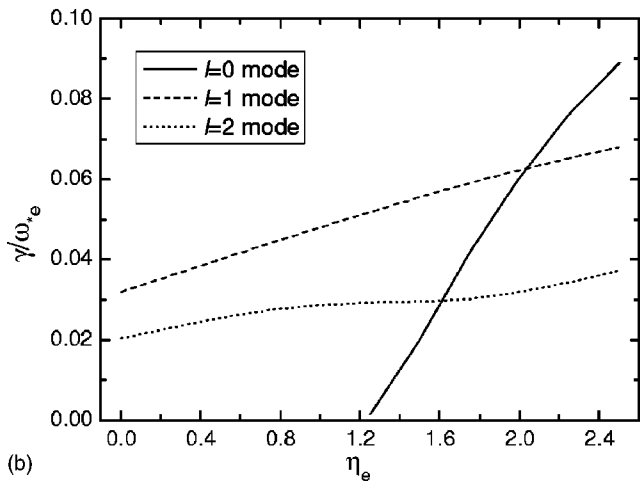
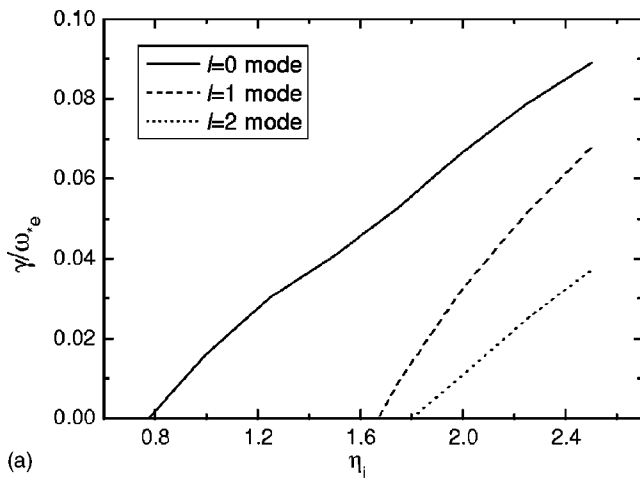


FIG. 3. (a) Normalized growth rates  $\gamma/\omega_{*e}$  vs  $\eta_i$  for fixed  $\eta_e=2.5$ ; (b)  $\gamma/\omega_{*e}$  vs  $\eta_e$  for fixed  $\eta_i=2.5$ ; (c) the stabilization diagram in the  $\eta_e$ - $\eta_i$  space, where the solid and dashed lines denote the critical stabilization boundary of the  $l=0$  and  $l=1$  modes, respectively, and the dotted line denotes the border where the  $l=0$  and  $l=1$  modes have same growth rates.  $k_\theta \rho_i=2$  and other parameters are the same as in Fig. 1.

the  $l=1$  mode. As a result, in the regions D and E, where  $\eta_e$  is relatively smaller than  $\eta_i$ , the  $l=1$  mode grows faster than the  $l=0$  mode and might be the dominant mode.

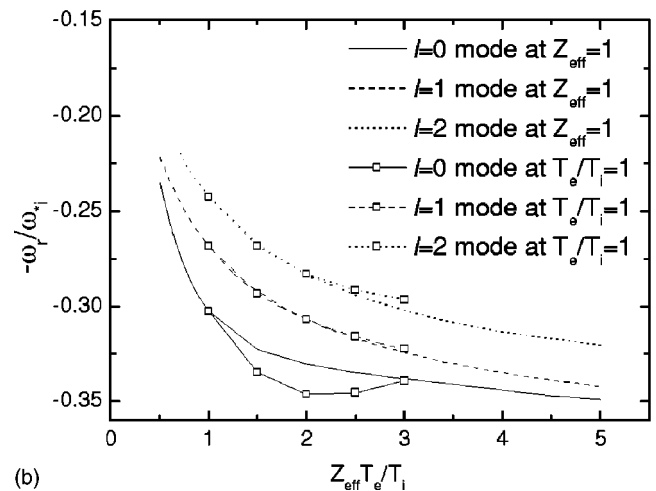
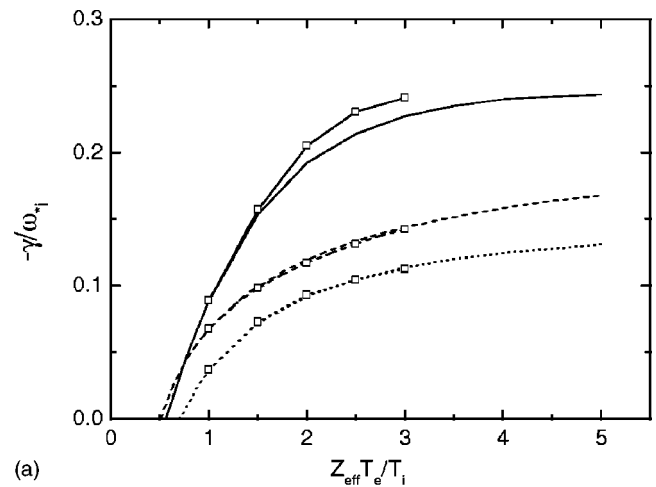


FIG. 4. Normalized growth rate (a) and frequency (b) vs  $Z_{eff} T_e/T_i$  for  $k_\theta \rho_i=2$ . The lines without squares are the results for  $Z_{eff}=1$  and the lines with squares are those for  $T_e/T_i=1$ . Other parameters and denotations are the same as in Fig. 1.

#### D. Dependence of temperature ratio, effective ion charges, and isotope mass

Figure 4 shows the mode frequency and growth rate normalized to  $|\omega_{*i}|$  vs  $T_e/T_i$  for  $k_\theta \rho_i=2$ . It is noted  $\omega_{*i}$  is negative in the definition in this paper. Same as the conventional ITG mode, the SWITG mode can be stabilized by hot ions (small  $T_e/T_i$ ). Here, we may distinguish two cases: varying  $T_e$  for fixed  $T_i$  and varying  $T_i$  for fixed  $T_e$ . Since the SWITG mode is dominated by the ion dynamics, the  $k_\theta$  corresponding to the maximum growth rate may follow the change in  $\rho_i$ . So  $k_\theta \rho_i=2$  is fixed and the  $k_\theta \rho_e$  varies with  $T_e/T_i$ .

In the adiabatic electron model, the ion effective charge is always accompanied the temperature ratio in the expression  $Z_{eff} T_e/T_i$ . Figure 4 shows the effect of  $Z_{eff}$  on the SWITG modes, which is roughly the same as the effect of  $T_e/T_i$ . It indicates again that ion response is dominant for the SWITG mode.

Figure 5 shows the isotope effect on the SWITG mode. The growth rate normalized to  $\omega_{*e}$  is insensitive to  $m_i/m_e$ , that is,  $\gamma/\omega_{*e} \sim \text{const}$ . However, it is noted that  $k_\theta \rho_i=2$  is fixed as mentioned in the discussion of the effect of tempera-

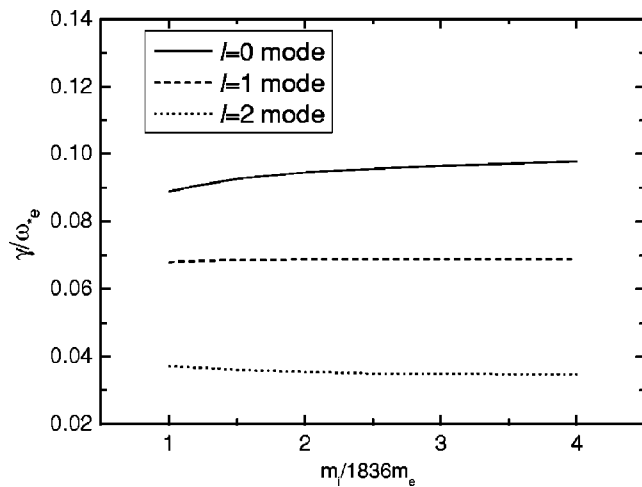


FIG. 5. Normalized growth rate vs  $m_i/m_e$  for  $k_\theta \rho_i = 2$ . Other parameters and denotations are the same as in Fig. 1.

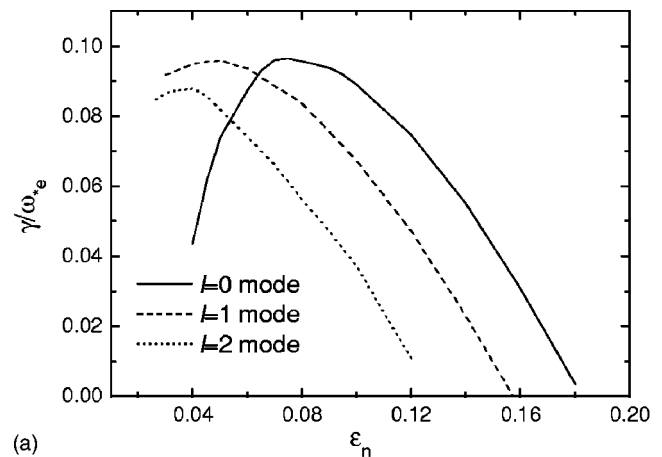
ture ratio. Since  $\omega_{*e} \propto k_\theta$  and  $\rho_i \propto m_i^{1/2}$ , the growth rate is proportional to  $m_i^{-1/2}$ . This isotope scaling from SWITG modes is also the same as that from conventional ITG modes.<sup>22</sup>

### E. $\epsilon_n$ variation

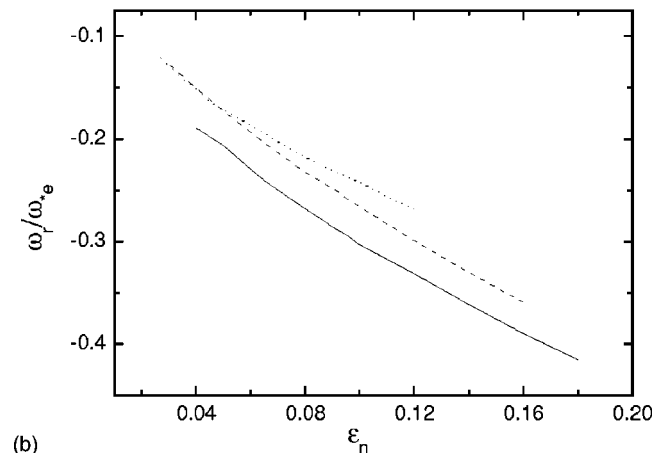
In Fig. 6, the normalized growth rate and real frequency as functions of  $\epsilon_n$  are shown. Hirose *et al.*<sup>19</sup> pointed out that the SWITG mode is essentially a slab mode. Indeed, the SWITG mode becomes stable at large  $\epsilon_n$  ( $>0.19$ ), where the conventional ITG persists unstable. It is because the  $\omega_{Di}$  increases with  $\epsilon_n$  and offers a stabilizing effect when  $\omega < \omega_{Di}$ . That is the same mechanism as the large  $k_\theta$  stabilization we discussed in Sec. III A. In fact, in the low  $\epsilon_n$  region, we can also see that the normalized growth rate increases with  $\epsilon_n$ , which implies the toroidal driving effect. The higher order modes are stabilized by smaller  $\epsilon_n$  since they have lower frequencies. It is noticed that both the  $l=1$  and  $l=2$  modes grow faster than the fundamental  $l=0$  mode in the low  $\epsilon_n$  region.

### F. Magnetic shear and safety factor variation

The magnetic shear effects are studied for both positive and negative shear and the results are shown in Fig. 7. First, the stabilizing effect of shear is confirmed, which is consistent with the results from the slab model<sup>18</sup> and also similar with other temperature gradient (ITG or ETG) driven modes. At weak positive shear, however, the growth rates of all three modes increase with the magnetic shear. Especially, the magnetic shear corresponding to the maximum growth rate of the fundamental mode is rather strong, about 1.5. It may be the reason why Hirose *et al.*<sup>19</sup> concluded that the SWITG is destabilized by magnetic shear, where the calculation region for magnetic shear is only from  $-1.0$  to  $1.5$ .<sup>19</sup> Second, the growth rate of the fundamental mode at negative shear is almost the same as that at positive shear. However, for  $l=1$  mode, obvious lower growth rate exists in negative shear regions and, even, no unstable  $l=2$  mode is founded in negative shear regions. Finally, the growth rate of the  $l=1$  mode



(a)



(b)

FIG. 6. Normalized growth rate (a) and frequency (b) vs  $\epsilon_n$  for  $k_\theta \rho_i = 2$ . Other parameters and denotations are the same as in Fig. 1.

is larger than that of the fundamental mode in the weak shear region, which is also similar to the behavior of slab SWITG modes.<sup>18</sup>

Dependence of the normalized growth rate and frequency on the safety factor is shown in Fig. 8. The fundamental mode shows the different behavior from the higher harmonic  $l=1$  and  $l=2$  modes. The fundamental mode becomes stable in the region  $q \gtrsim 3.0$ . It may be explained by the contribution of electron parallel dynamics, for the transit frequency ( $\sim v_{te}/qR$ ) decreases with  $q$  increasing. Since the  $l=1$  and  $l=2$  modes have lower frequencies, the growth rates of them tend to be constant at high  $q$ . However, in finite  $\beta$  plasmas, a large  $q$  is expected to be stabilizing the modes through  $\alpha(-q^2 R d\beta/dr)$  stabilization.

### G. Finite $\beta$ stabilization

Figure 9 shows the  $\beta$  dependence of mode growth rate and frequency. Finite  $\beta$  influences the mode by two ways: one is coupling to Alfvén waves; the other is influencing the toroidal drift frequency through the ballooning parameter  $\alpha(-q^2 R d\beta/dr)$ . The lines with squares are the results from the electrostatic model, Eq. (6) alone, but the effect of  $\alpha$  is retained. The mode growth rates increase slightly when  $\beta$  increases from zero to a certain value, but a further increase in  $\beta$  causes the decrease in the growth rate. Since the funda-

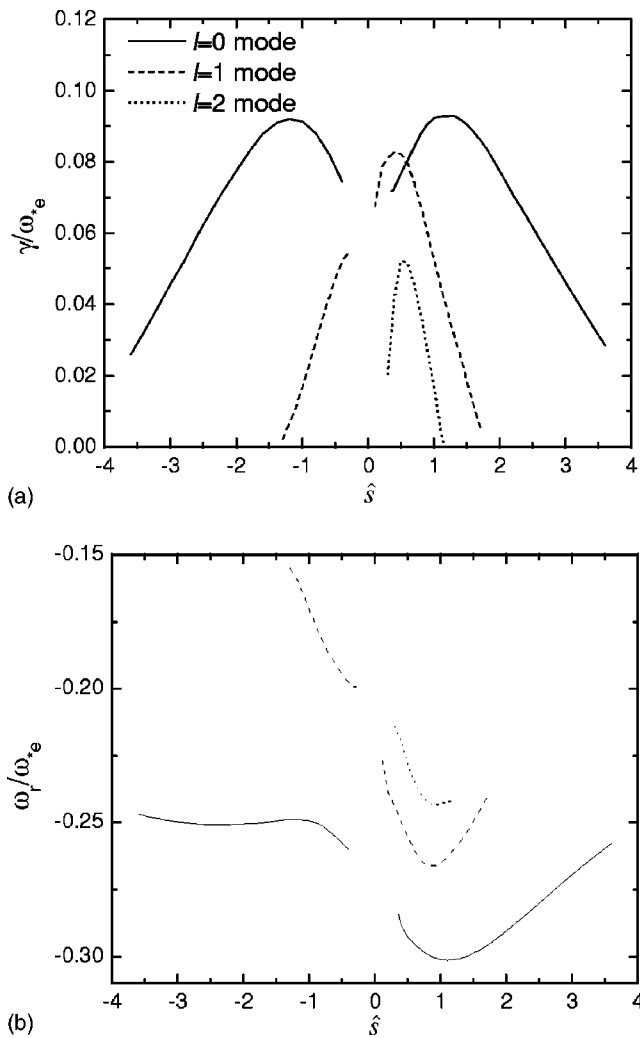


FIG. 7. Normalized growth rate (a) and frequency (b) vs  $\hat{\delta}$  (positive and negative) for  $k_{\perp}\rho_i=2$ . Other parameters and denotations are the same as in Fig. 1.

mental mode has a higher frequency, it has a stronger ability to satisfy the toroidal drift resonance condition. The numerical result shows the growth rate of the fundamental mode is slightly influenced by this pure  $\alpha$  effect. However, the coupling effect to shear Alfvén waves (SAWs) is also important at finite  $\beta$ . The lines without symbols are the results from the model with both the coupling effect to SAWs ( $\tilde{A}_{\parallel}$ ) and the effect of  $\alpha$  inclusion. The fundamental mode is easily stabilized by finite  $\beta$ , which is consistent with the result from Hirose *et al.*<sup>19</sup> Contrastively, the higher order modes are more hardly stabilized than the fundamental mode. It might be explained by the fact that the higher order modes have lower frequencies. A conclusion is that, in the study<sup>23</sup> of the slab ITG mode with the coupling to SAWs, the  $\beta$  cannot effectively change the frequency and growth rate of the mode with very low frequency. Physically, the frequency of the SWITG modes for the present parameters is lower than the frequency of the SAWs,  $\omega_A \sim v_A/qR = v_{ti}/(qR\sqrt{\beta_i})$ , where  $v_A$  is the Alfvén velocity, so the coupling to SAWs will influence the fundamental mode with higher frequency more. However, it is noted that, in the sheared slab configuration,

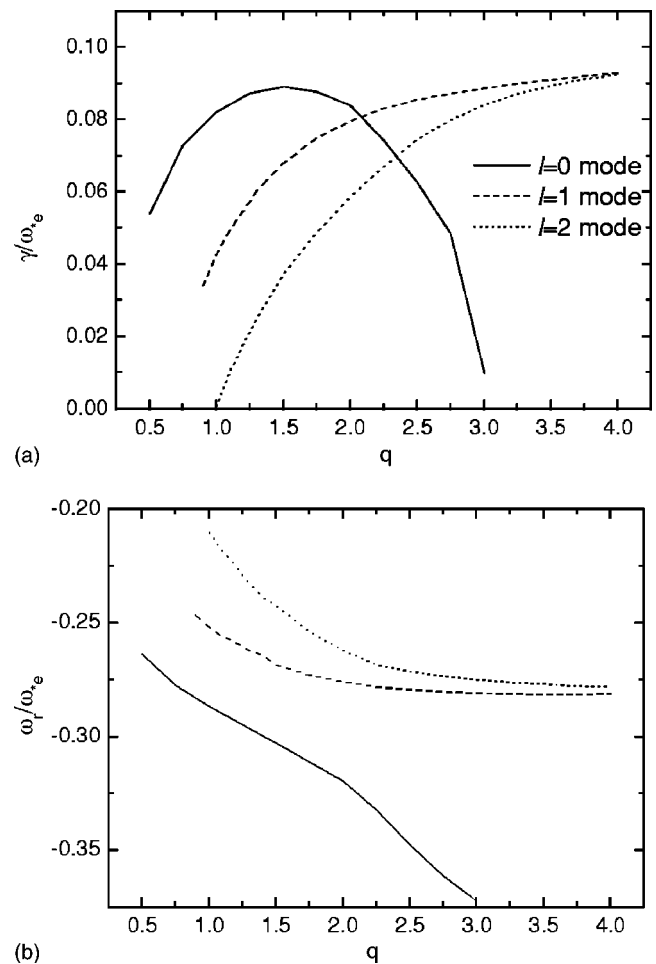


FIG. 8. Normalized growth rate (a) and frequency (b) vs  $q$  for  $k_{\perp}\rho_i=2$ . Other parameters and denotations are the same as in Fig. 1.

the fundamental mode has a lower frequency and more hardly to be stabilized by  $\beta$  than the  $l=1$  mode.<sup>18</sup>

#### IV. CONCLUSIONS AND DISCUSSION

In this paper, several unstable branches of temperature gradient driven modes in the short wavelength region,  $|k_{\perp}\rho_i| > 1$ , are identified with a gyrokinetic integral equation code in toroidal plasmas, which include the fundamental even ( $l=0$ ) mode, an odd ( $l=1$ ) mode and a higher order even ( $l=2$ ) mode. These modes propagate in the ion diamagnetic direction and have almost the same growth rate as the corresponding conventional ITG modes. These unstable modes still exist even if electrons are adiabatic, so-called SWITG modes. At typical parameters, excitation of the fundamental mode requires that both  $\eta_i$  and  $\eta_e$  exceed thresholds, while the higher order modes only require finite  $\eta_i$  and persist unstable even at  $\eta_e=0$ . As a result, the  $l=1$  mode dominates in the region with relatively low  $\eta_e$ . If nonadiabatic electron response is included, the SWITG modes have wide and oscillatory eigenfunctions along the field line.

Parameter dependence of the SWITG modes is investigated in detail. A decrease in temperature ratio ( $T_e/T_i$ ) can stabilize the modes, which is similar to the behavior of the conventional ITG modes. Toroidicity shows a stabilizing ef-

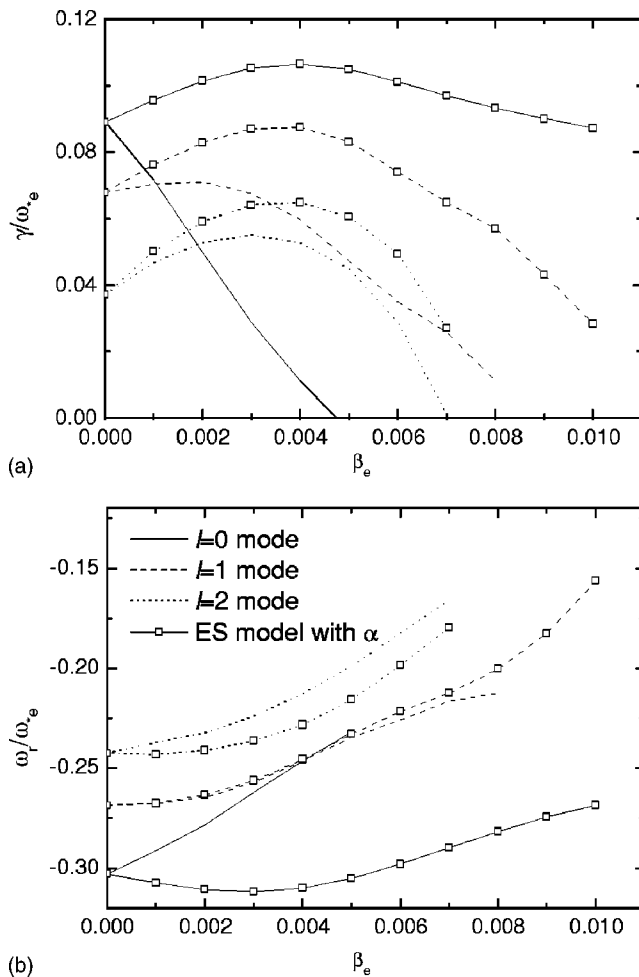


FIG. 9. Normalized growth rate (a) and frequency (b) vs  $\beta_e$  for  $k_{\theta}\rho_i=2$ . The lines with squares are the results from Eq. (6) alone, but  $\alpha$  is retained. The other parameters and denotations are the same as in Fig. 1.

fect on the SWITG mode when the toroidal drift frequency is apart from the resonance region. Although the growth rate of the fundamental mode increases with magnetic shear in weak and medium shear regions, strong magnetic shear can stabilize the mode. The  $l=1$  mode with an odd eigenfunction grows faster than the fundamental mode in weak magnetic shear regions. The growth rate of the fundamental mode at negative shear is almost the same as that at positive shear, while the higher order modes have lower growth rate at negative shear than at positive shear. The fundamental mode seems more easily to be stabilized by finite  $\beta$  than the higher order modes with lower frequencies due to the coupling effect to sheared Alfvén waves.

Hirose *et al.*<sup>18</sup> has already confirmed and investigated the fundamental SWITG modes at low beta. Some conclusions are similar as the results shown in this paper, and some are improved through wider parameter scan, for example, the magnetic shear stabilization effect. Moreover, the physical mechanism is discussed according to analytical and numerical results. The ion response is essential for the SWITG mode. The toroidal SWITG mode has a similar physical mechanism as the slab mode, except that the toroidal drift resonance plays an important role instead of the Landau

resonance. Also, high order modes are investigated in this paper and it is found that the  $l=1$  SWITG mode grows faster and maybe dominate in such cases as high  $\beta$ , flat electron temperature profile (low  $\eta_e$ ), weak positive magnetic shear and/or weak toroidicity.

Considering the possibility of the SWITG instability as a candidate to explain electron transport is necessary. It is naturally considered that the SWITG mode has a longer wavelength and then can induce higher transport than the ETG mode.<sup>17</sup> However, we cannot curly derive the characteristic radial scale length from the eigenfunction in the ballooning space unless we go into the two-dimension work. Early studies<sup>24</sup> introduced the radial-variation component of the eikonal,  $S(x)$  (sometimes written in terms of the radial Fourier transform wave number  $k_{x0}$  or the ballooning angle label  $\theta_0$ ) to describe the two-dimension structure of eigenmodes. The total radial wave number is composed of two parts,  $k_x = k_{x0} + k_{\rho}\hat{s}\theta \equiv k_{\rho}\hat{s}(\theta - \theta_0)$ , so the radial structure of the eigenmode in the real space depends on not only the  $\theta$  spectrum but also the choice of  $\theta_0$ . Results in Sec. III B show that the nonadiabatic electrons strongly modify the mode structure with oscillatory profile at  $\theta_0=0$ , which induces a dramatic increase in the spectral width in the  $\theta$  space. Moreover, the mechanism of the nonadiabatic electron effect seems to be irrelative to  $\theta_0$ . Therefore, nonadiabatic electrons might cause a decrease in the radial scale length of the unstable eigenmode, which implies the reduction of thermal conductivity due to non-adiabatic electrons. However, this is an open issue and a further and more careful investigation is needed.

The electric field shear, or  $V'_E$ , stabilization of the slab SWITG has been studied.<sup>25</sup> Since the SWITG mode has a lower frequency than the conventional ITG mode in the sheared slab configuration, a lower  $V'_E$  is needed to stabilize the slab SWITG mode than that to stabilize the slab conventional ITG mode. The physical mechanism is that, when the mode frequency is lower, the  $V'_E$  more easily changes the argument of the plasma dispersion function,  $\xi = (\omega - k_y V'_E x) / k_{\parallel} v_r$ . If this mechanism is still valid in the toroidal geometry, the toroidal SWITG mode might more hardly be stabilized with  $\mathbf{E} \times \mathbf{B}$  flow shear than the toroidal conventional ITG mode might be. It has mentioned in Fig. 1 that the toroidal SWITG mode has a higher frequency than the toroidal conventional ITG mode.

However, it seems that the SWITG mode depends upon the ion dynamics much although the fundamental SWITG mode also has a  $\eta_e$  threshold. Indeed, some experiments show the correlation between ion transport and electron transport. Especially, in TFTR the measured fluctuations responsible for anomalous electron transport propagate in the ion diamagnetic direction ( $\omega_r < 0$ ) and with  $k_{\perp}\rho_i \sim 5$ , which agrees with the behaviors of the SWITG mode. However, in some ECH plasmas where electron dynamics are decoupled from ion dynamics, the SWITG mode seems hardly to be excited. Anyway, the SWITG instability provides a possible channel of electron transport. Further investigation is needed, especially the critical electron temperature gradient at different temperature ratio and different ion temperature profile. This work will be performed soon.

## ACKNOWLEDGMENTS

The useful discussion with Dr. H. Sugama is gratefully acknowledged.

One of the authors (Z.G.) is grateful for the hospitality by many staff members during his visit at the National Institute for Fusion Science, Japan. His work was supported by the Visiting Professorship from Japanese Ministry of Education, Science and Culture and by the Improving Tsinghua to Top-ranking University Fund. This work was also partly supported by the National Natural Science Foundation of China (NSFC) under Grant Nos. 10405014 and 10135020.

- <sup>1</sup>F. Ryter, C. Angioni, M. Beurskens *et al.*, *Plasma Phys. Controlled Fusion* **43**, A323 (2001).  
<sup>2</sup>V. V. Parail, *Plasma Phys. Controlled Fusion* **44**, A63 (2002).  
<sup>3</sup>A. Fujisawa, H. Iguchi, T. Minami *et al.*, *Phys. Plasmas* **7**, 4102 (2000).  
<sup>4</sup>K. Itoh, *Nucl. Fusion* **43**, 1710 (2003).  
<sup>5</sup>G. D. Conway, D. N. Borba, B. Alper *et al.*, *Phys. Rev. Lett.* **84**, 1463 (2000).  
<sup>6</sup>K. L. Wong, N. L. Bretz, T. S. Hahm, and E. Synakowski, *Phys. Lett. A* **236**, 339 (1997).  
<sup>7</sup>C. M. Greenfield, K. H. Burrell, T. A. Casper *et al.*, *Proceeding of the 27th EPS Conference on Controlled Fusion and Plasma Physics*, Budapest, 2000, edited by K. Szegő, T. N. Todd, and S. Zoletnik (European Physical

- Society, Petit-Lancy, 2000), Vol. 24B, p. 544.  
<sup>8</sup>J. Weiland, A. Jarmen, and H. Nordman, *Nucl. Fusion* **29**, 1810 (1989).  
<sup>9</sup>H. Nordman, J. Weiland, and A. Jarmen, *Nucl. Fusion* **30**, 983 (1990).  
<sup>10</sup>K. H. Burrell, *Phys. Plasmas* **4**, 1499 (1997).  
<sup>11</sup>J. Q. Dong, G. D. Jian, A. K. Wang, H. Sanuki, and K. Itoh, *Nucl. Fusion* **43**, 1185 (2003).  
<sup>12</sup>F. Jenko, W. Dorland, and G. W. Hammett, *Phys. Plasmas* **8**, 4096 (2001).  
<sup>13</sup>J. Q. Dong, H. Sanuki, K. Itoh, and Liu Chen, *Phys. Plasmas* **9**, 4699 (2002).  
<sup>14</sup>F. Jenko, W. Dorland, M. Kotschereuther, and B. N. Rogers, *Phys. Plasmas* **7**, 1904 (2000).  
<sup>15</sup>W. Horton, G. T. Hoang, C. Bourdelle *et al.*, *Phys. Plasmas* **11**, 2600 (2004).  
<sup>16</sup>F. Ryter, G. Tardini, F. De Luca *et al.*, *Nucl. Fusion* **43**, 1936 (2003).  
<sup>17</sup>A. I. Smolyakov, M. Yagi, and Y. Kishimoto, *Phys. Rev. Lett.* **89**, 125005 (2002).  
<sup>18</sup>Z. Gao, H. Sanuki, K. Itoh, and J. Q. Dong, *Phys. Plasmas* **10**, 2831 (2003).  
<sup>19</sup>A. Hirose, M. Elia, A. I. Smolyakov, and M. Yagi, *Phys. Plasmas* **9**, 1659 (2002).  
<sup>20</sup>J. Q. Dong, L. Chen, and F. Zonca, *Nucl. Fusion* **39**, 1041 (1999).  
<sup>21</sup>J. Q. Dong, W. Horton, and J. Y. Kim, *Phys. Fluids B* **4**, 1867 (1992).  
<sup>22</sup>J. Q. Dong, W. Horton, and W. Dorland, *Phys. Plasmas* **1**, 3635 (1994).  
<sup>23</sup>Z. Gao, J. Q. Dong, G. J. Liu, and C. T. Ying, *Phys. Plasmas* **9**, 569 (2002).  
<sup>24</sup>G. Rewoldt, W. M. Tang, and E. A. Frieman, *Phys. Fluids* **21**, 1513 (1978).  
<sup>25</sup>Z. Gao, J. Q. Dong, and H. Sanuki, *Phys. Plasmas* **11**, 3053 (2004).